Available online at www.sciencedirect.com
ScienceDirect
Journal of Food Engineering xxx (2008) xxx–xxx
JOURNAL OF FOOD ENGINEERING
www.elsevier.com/locate/jfoodeng

Heat transfer analysis of canned food sterilization in a still retort

A. Kannan *, P.Ch. Gourisankar Sandaka [1]

Department of Chemical Engineering, Indian Institute of Technology Madras, Chennai 600 036, India

Received 6 February 2007; received in revised form 3 December 2007; accepted 6 February 2008

Abstract

Computational fluid dynamics (CFD) analyses provide insight on the natural convective processes occurring during the sterilization of canned liquid food. The definition and estimation of heat transfer coefficients pertaining to the transient heat transfer occurring in cylindrical food cans is presented. The heat transfer coefficients defined on the basis of absolute mass flow averaged and volume-averaged temperatures are compared. The contributions to the overall heat transfer rate from different surfaces of the uniformly heated cylindrical can are evaluated. The influence of the temperature difference to viscosity ratio on the peculiar Nusselt number trends is discussed. Unified correlations are provided for the Nusselt number as functions of Fourier number, food can aspect ratio and thermal conductivity of the food medium in both the conduction and convection dominated heat transfer regimes.

Keywords: Thermal food sterilization; Heat transfer coefficients; Natural convection

1. Introduction

Liquid food material is often sterilized in still retorts with steam flowing around the surface of the can. This food is sterilized mainly by natural convection when vigorous agitation is ruled out. Such situations may arise during in-package pasteurization of liquids in bottles. Further, agitation equipment may not be justified when liquid food is processed in low volumes. Food sterilized in cans include in-packaged heat pasteurized beer, evaporated milk, thin soups and broth, pureed vegetables, fruit and vegetable juices and vegetable soups (Datta and Teixeira, 1988; Kumar et al., 1990). It is important to develop better understanding of the heat transfer phenomena that are associated with the thermal sterilization process from the viewpoint of improving its design and operation. This work focuses on the definition and direct estimation of heat transfer coefficients obtained during the sterilization process from CFD simulations. Unified Nusselt number correlations are drawn from CFD simulations on heat transfer in food cans with different aspect ratios and food medium thermal conductivities.

2. Background and scope

Engelman and Sani (1983) studied the pasteurization of beer in glass bottles through finite element simulations. Datta and Teixeira (1988) presented transient flow and temperature patterns estimated from numerical simulations of natural convective heat transfer occurring in a uniformly heated can. Zechman and Pflug (1989) analyzed the influence of medium properties and metal container size on the location of slowest heating zone (SHZ) in canned media. Kumar et al. (1990) numerically simulated the natural convection in canned thick viscous liquid food heated through the sidewall. Kumar and Bhattacharya (1991) simulated the sterilization of pseudoplastic liquid food, which was heated from all sides. Ghani et al. (1999) carried out transient numerical simulations of natural convective heating process in canned food sterilization and analyzed the slowest heating zone characteristics. Ghani et al. (2002a)

* Corresponding author. Tel.: +91 044 2257 4170; fax: +91 044 2257 0545.
E-mail address: kannan@iitm.ac.in (A. Kannan).
[1] Cognizant Technology Solutions, Chennai.

0260-8774/$ - see front matter © 2008 Elsevier Ltd. All rights reserved.
doi:10.1016/j.jfoodeng.2008.02.007

Nomenclature

AARD	average absolute relative deviation
C_p	specific heat of the liquid in the can, J/ kg °C
C_{nc}	natural convection constant
CMC	carboxy-methyl cellulose
D	diameter of can, m
E_a	activation energy, kJ kg^{-1} mol
Fo	Fourier number
Fo_1	Fourier number during transient period
g	gravitational acceleration constant, m/s^2
Gr	Grashof number
Gr_{VP}	Grashof number for a vertical plate
h	heat transfer coefficient, W/m^2 °C
h^M	local heat transfer coefficient based on absolute mass flow average temperature, W/m^2 °C
h^V_{avg}	volume averaged heat transfer coefficient, W/ m^2 °C
h_{total}	specific total enthalpy, J/kg
J_0	zero-order Bessel function
J_1	first-order Bessel function
k	thermal conductivity of the liquid in the can, W/ m °C
k_e	effective thermal conductivity of liquid food in the can, W/m °C
K	fluid consistency index, Pa s^n
L	height of the can or length of vertical plate, m
n	exponent to shear rate in dynamic viscosity expression
Nu	Nusselt number
Nu_c	Nusselt number in conduction dominated regime
Nu_{hc}	Nusselt number for a horizontal cylinder
Nu_{max}	maximum Nusselt number
Nu_r	reduced Nusselt number
Nu_S	aspect ratio scaled Nusselt number
Nu^*_S	aspect ratio scaled Nusselt number predicted from theory
Nu_{VP}	mean Nusselt number for a vertical plate
Pr	Prandtl number
Pr_{VP}	Prandtl number for a vertical plate
q_w	wall heat flux, W/m^2 °C
Q	heat transfer rate, W
r	radial coordinate
R	radius of the can, m
Ra	Rayleigh number
Ra_d	Rayleigh number based on diameter
Ra_{d0}	Rayleigh number calculated for the initial time
Ra_r	reduced Rayleigh number
Ra_{max}	maximum Rayleigh number
S	aspect ratio
S_M	source term for momentum
S_E	source term for energy
SHZ	slowest heating zone
t	time of heating, s
T	temperature, °C
T_0	initial temperature inside food can, °C
T_{wall}	temperature at the wall of the can, °C
$\langle T^M \rangle$	absolute mass flow averaged temperature, °C
$\langle T_i \rangle$	initial volume-averaged temperature, °C
$\langle \overline{T}^M \rangle$	axially averaged absolute mass flow averaged temperature, °C
$\langle T^V \rangle$	volume average temperatured, °C
V	velocity vector
V_r	velocity in the radial direction, m/s
V_z	velocity in the axial direction, m/s
z	axial coordinate
Z	axial distance, m

Greek letters

α_T	thermal diffusivity, m^2/s
β	thermal expansivity, K^{-1}
γ	rate of shear, s^{-1}
γ_n	nth root of the zero-order Bessel function
δ	Kroneckar delta
μ	apparent viscosity, Pa s
μ_o	consistency index, Pa s^n
μ_{ref}	characteristic viscosity, Pa s^n
$\langle \mu \rangle$	volume averaged viscosity, Pa s
ρ	density, kg/m^3
θ	azimuthal coordinate
$\langle \Delta T \rangle$	volume averaged temperature difference, °C

studied both experimentally and numerically the thermal deactivation of bacteria in food pouches. In another study, Ghani et al. (2002b) presented simulation and experimental results on the thermal destruction of vitamin C in food pouches. Subsequently, Ghani et al. (2002c) investigated thermal sterilization of carrot–orange soup in a horizontally oriented cylindrical can. Ghani et al. (2003) investigated the thermal sterilization rate when the can containing viscous carrot–orange soup was rotated at 10 rpm. The combined natural and forced convection was observed to split the slowest heating zone into two regions. Varma and Kannan (2005, 2006) investigated the effects of modifying the geometry of the conventional cylindrical food can as well as the can's orientation on the rate of thermal sterilization of pseudoplastic food from CFD simulations. A cone pointing upwards was found to heat faster than the cylinder of equal volume while the cone pointing downward heated the slowest.

Accurate measurement of temperatures inside the can undergoing thermal treatment is difficult because probes may disturb the temperature-velocity fields. Further, the slowest heating zone is not fixed at one location (Ghani

Please cite this article in press as: Kannan, A., Sandaka, P.C.G., Heat transfer analysis of canned food sterilization in a still retort, Journal of Food Engineering (2008), doi:10.1016/j.jfoodeng.2008.02.007

et al., 2002a). For this reason, mathematical modeling approach has been extensively applied to predict the temperature patterns in the thermal sterilization process (Teixeira et al., 1969; Naveh et al., 1983; Datta and Teixeira, 1987, 1988; Nicolai et al., 1998; Farid and Ghani, 2004). Even in the relatively simpler conductive heat transfer study using temperature sensors, Marra and Romano (2003) observed that the sensor presence, location and size relative to the can dimensions influenced the estimated cold spot temperature evolution and sterility values. They further noted that the sterility time calculations should incorporate a safety factor when temperature sensors are used especially in small cans.

Earlier studies have mainly focused on temperature-velocity-concentration profiles, location and movement of the slowest heating zone and effects of geometry modifications, motion and orientation. However, for a natural convection dominated heat transfer problem, knowledge of the fundamentally important heat transfer coefficients is required. In the literature, natural convective heat transfer coefficients have been mainly recorded for flows past single infinitely long heated walls, parallel walls at different temperatures and inclined plates. In the case of heated cylinders or spheres, the flow domain external to the heated surface has been mainly studied. Rectangular cavities, concentric cylinders and spheres maintained at different temperatures have also been investigated (Dewitt and Incropera, 2001).

Relatively little work appears to have been carried out in the case of isothermal cylindrical cans such as those encountered in food sterilization. Farid and Ghani (2004) observed that a correlation for predicting heat transfer coefficient is not available for liquids contained in vertical and horizontal cans. These authors proposed a technique for calculating sterilization times. Using the simplified classical solution for transient heat transfer in infinitely long cylinders, they attempted to predict the slowest heating zone temperature. The slowest heating zone temperature was used in the definition of the dimensionless temperature. An effective thermal conductivity (k_e) was used in the thermal diffusivity term to factor in the contribution from natural convection. The heat transfer coefficient correlation developed by Catton (1978) for parallel vertical walls that were maintained at different temperatures was applied. The authors justified this approach on the basis that the natural convection induced circulation rolls were similar to those observed in cylindrical cans. However, in the cylindrical can situation, while the outer wall temperature is constant, the axis temperature is varying from top to bottom.

In a recent work, Martynenko and Khramtsov (2005) reviewed Nusselt number correlations for natural convection in cylindrical enclosures. These authors summarized transient two dimensional heat transfer results inside a completely filled horizontal cylinder at aspect ratios exceeding 2.5. Correlations were proposed for Nusselt number as functions of Rayleigh number and Fourier number in the transient period. The involved nature of these correlations testifies to the complex nature of the phenomena occurring inside the cylinder. However, this work does not indicate the methodology through which the heat transfer coefficients were estimated.

In the present work, the methodology for estimating the heat transfer coefficient directly from the CFD data is illustrated. The temperature driving force used in the heat transfer coefficient has to be properly defined and two of these definitions are compared. The contributions to the overall heat transfer rate from the different surfaces of the food can are compared. Unified correlations are drawn for the Nusselt number for different can aspect ratios and food medium thermal conductivities. This study focuses on the heating cycle involving steam. In a recent study, Ghani (2006) has also analyzed the cooling cycle of the food sterilization process using CFD.

3. Details of food systems and can geometry

The pseudo plastic fluid involving 0.85% w/w CMC solution in water was taken as the model system. The properties of this system given in Table 1 were based on the study of Kumar and Bhattacharya (1991). Steffe et al. (1986) suggested that this model to be applicable for tomato puree, carrot puree, green bean puree, applesauce, apricot and banana purees, which are regularly canned and preserved usually by heating. For validating the CFD calculations, experiments were also conducted. Commercial CMC (LR grade) was procured from Sdfine-Chem Limited, Mumbai and a 0.85% w/w solution was prepared. This experimental system was characterized by the Anton Paar cone and plate Rheometer (Physica MCR 301) of the high polymer-engineering laboratory of IIT Madras. The power law parameters for this solution are also included in Table 1 (Neeharika, 2007). Other listed properties are taken to be the same for both systems.

For aiding the development of correlations, a range of thermal conductivities (0.35–1.4 W/m °C) and food can aspect ratios (1.37–2.37) were considered in this study. Two standard cylindrical cans (Can Manufacturers Institute, Washington) were used in the analysis. The cans were

Table 1
Properties of the model and experimental food system

System properties	Value/expression	Units
Viscosity (μ)	$\mu = \mu_o \exp\left(\frac{nE_a}{RT}\right)\dot{\gamma}^{n-1}$	Pa s
Consistency index (μ_0)	0.002232 (model system) 1.411×10^{-5} (experimental system)	Pa s^n
Activation energy (E_a)	30.74×10^3	J/g mol
Parameter for shear rate, n	0.57 (model system) 0.82 (experimental system)	–
Specific heat (C_p)	4100	J/kg °C
Thermal conductivity (k)	0.7	W/m °C
Density (ρ_{ref})	950	kg/m^3
Coefficient of volume expansion (β)	0.0002	$°C^{-1}$

Please cite this article in press as: Kannan, A., Sandaka, P.C.G., Heat transfer analysis of canned food sterilization in a still retort, Journal of Food Engineering (2008), doi:10.1016/j.jfoodeng.2008.02.007

Table 2
Details of food cans used in the CFD simulations

Can label	D (m)	L (m)	S (–)	Mesh volume $\times 10^{10}$ (m^3)		Number of hexahedral elements used for simulations
				Minimum	Maximum	
Regular	0.081	0.111	1.37	0.64	5.64	55,000
Medium	0.068	0.124	1.81	1.06	10.0	127,500
Long	0.065	0.150	2.31	3.62	20.3	201,600

labeled on the basis of their aspect ratios. The can labeled as 'Regular' has been commonly used in previous studies (Kumar and Bhattacharya, 1991; Ghani et al., 1999; Varma and Kannan, 2005, 2006). The simulations based on this can are used to illustrate the analysis of heat transfer coefficients in Section 5. Further, a non-standard can dimension labeled 'Long' was also included in the analysis for studying the effects of parameters. The details of the cans used in the simulations are given in Table 2.

4. Experimental procedure

Experiments were carried out with the regular can (Neeharika, 2007). Openings were drilled into the top surface of the food can and Teflon plugs were inserted into these holes to fit the 3 mm diameter thermocouples vertically. A thermocouple was used to measure the temperature at the midpoint of the can. The food can was housed within a cylindrical chamber. The cylindrical chamber was made of stainless steel (grade 304) with an internal ring support to hold the food can vertically. The can was held above the chamber base to ensure that the steam flowed freely on all sides around the can. A flanged arrangement was welded to the cylindrical body of the chamber so that the lid could be tightly bolted. A rubber gasket was used between the flanges to ensure that the chamber was leak proof. A thermocouple was used to monitor the steam temperature in the chamber during the course of the experiments. After the top flange was bolted to the cylinder base, the steam line was activated. At the start of the run, the steam outlet port at the top was partially opened and subsequently controlled with minor adjustments to maintain steam temperature at 121 °C. After the temperatures in the can reached constant values, the steam line was deactivated and the condensate drained off the chamber. The reproducibility of the midpoint temperature measurements were found to be within ±3%.

5. Governing equations and numerical solution methodology

The commercial CFD package CFX v5.7, which is based on the finite volume method, was used to solve the governing transport equations for the defined geometry and associated boundary conditions. The domain was defined in the global co-ordinate frame. A non-staggered collocated grid is used. The continuity equation is modified in an extension to the scheme adopted by Rhie and Chow (1983). This enables overcoming of checkerboard oscillations in pressure and velocity associated with collocation. The linear sets of equations that arise after discretization are solved in a coupled fashion, thereby avoiding segregation. This method ensures robustness, efficiency and simplicity at the cost of high storage of all the coefficients.

5.1. Transport equations

The generalized transport equations that were solved in CFX (2003) are

(a) Continuity equation

$$\frac{\partial \rho}{\partial t} + \nabla \cdot (\rho V) = 0 \tag{1}$$

(b) Momentum equation

$$\left(\frac{\partial \rho V}{\partial t} + \nabla \cdot (\rho V \otimes V)\right) = \nabla \cdot (-p\delta + \mu(\nabla V + (\nabla V)^t)) + S_M \tag{2}$$

(c) Energy equation

$$\left(\frac{\partial \rho h_{total}}{\partial t} - \frac{Dp}{Dt} + \nabla \cdot (\rho V h_{total})\right) = \nabla \cdot (k \nabla T) + S_E \tag{3}$$

In Eq. (3) h_{total} is defined as the specific total enthalpy.

In CFX, the momentum source term S_M is defined by

$$S_M = (\rho - \rho_{ref})g \tag{4}$$

Applying the Boussinesq approximation, the body force term (S_M) hence becomes

$$S_M = -\rho_{ref}\beta(T - T_{ref})g \tag{5}$$

When this form is used, the pressure in the momentum equation excludes the hydrostatic contribution from ρ_{ref} (CFX, 2003). As there are no internal sources of energy, S_E is taken to be zero. A material termed CMC was created in the pre-processor library and its properties were specified in accordance with Table 1. It is assumed that the flow involves an incompressible high viscous liquid with negligible viscous dissipation effects. Based on the properties defined, the software uses an inbuilt mechanism for generating enthalpy variations with temperature.

5.2. Boundary and initial conditions

Ghani et al. (1999) suggest that simulations based on uniform heating on all sides of the can with constant wall temperature are appropriate for a general purpose. All walls of the enclosure are kept at 121 °C with the cylinder placed in an upright position. At the curved wall of the can, no slip conditions apply with specified temperatures

$$T = T_{wall} = 121\ ^\circ\text{C}, \quad V_r = 0\ \text{m/s}, \quad V_z = 0\ \text{m/s}$$
$$\text{for } 0 \leqslant z \leqslant L \text{ at } r = R$$

Please cite this article in press as: Kannan, A., Sandaka, P.C.G., Heat transfer analysis of canned food sterilization in a still retort, Journal of Food Engineering (2008), doi:10.1016/j.jfoodeng.2008.02.007

At the top and bottom walls of the container, again no slip conditions apply with specified temperatures

$$T = T_{\text{wall}} = 121\ ^{\circ}\text{C}, \quad V_r = 0\ \text{m/s}, \quad V_z = 0\ \text{m/s}$$
$$\text{for } 0 \leqslant r \leqslant R \text{ at } z = 0 \text{ and } L$$

Initially the fluid is at rest and at a uniform initial temperature

$$T_0 = 40\ ^{\circ}\text{C}, \quad V_r = 0\ \text{m/s}, \quad V_z = 0\ \text{m/s}$$
$$\text{for } 0 \leqslant r \leqslant R \text{ and } 0 \leqslant z \leqslant L$$

The condensing steam is assumed to maintain a commonly applied constant temperature of 121 °C at all boundaries. This temperature is assumed to apply at the liquid boundaries owing to the very small thermal resistance of the can material. Further, the temperature at the liquid boundaries is assumed to reach this temperature from the initial conditions without any lag.

5.3. Mesh and time step details

CFD simulations, especially those involving transients, are time consuming even with faster processors. Exploiting the axisymmetry, only a segment of the cylinder was used. The structured mesh option from CFX Build v 5.6 was applied. To resolve the rapid changes in velocities and temperatures near the walls, finer rectangular mesh was applied closer to the walls, which gradually gave way to increasingly coarser ones towards the core. For the cylinders used in the study, the smallest element size was around 0.3 mm, while the largest element size was near 1 mm in the radial direction. Along the axial direction, the mesh sizes were between 1 and 2 mm. The total number of hexahedral elements in the domain and mesh volumes for each case is included in Table 2. The transient runs were carried out by adopting the step size-time relationship provided by Kumar and Bhattacharya (1991). Upon doubling the time step sizes, the results did not differ significantly. However, the earlier finer time step strategy was chosen.

The results from the structured meshes used here compared well with the earlier reported values for midpoint temperatures of Kumar and Bhattacharya (1991) as well as from Varma and Kannan (2005). The unstructured mesh scheme was used by Varma and Kannan (2005, 2006) in their previous studies. A coarse structured mesh scheme was also investigated in the present work to study the effect of mesh sizes. For instance, a coarse mesh scheme was tested for the regular cylinder with 25,000 hexahedral elements as against 55,000 hexahedral elements used in the fine mesh scheme. The element sizes were roughly 1.9 times higher along the radial direction with the minimum and maximum mesh sizes being 0.6 mm and 2.3 mm. The results were not found to be in significant variance. However, the refined mesh scheme whose details were shown in Table 2 was used in this work.

Finally, the axisymmetry condition was also verified by simulating over the entire cylinder. No significant azimuthal flow or variations in temperatures were encountered. Detailed results of mesh independency studies are provided elsewhere (Gourisankar, 2006). The simulations were executed in the Intel Pentium (R) 4, 3.06 GHz and 1 GB RAM with Windows XP platform. The CPU time for the regular cylinder case for instance was estimated at 1.2 h.

5.4. Solution methodology

The transient calculations were carried out using the robust and bounded first-order backward Euler scheme. CFX has the optional schemes of first order upwind difference and numerical advection with specified blend factor. The blend factor may be varied between 0 and 1 to opt between the first- and second-order schemes in order to control numerical diffusion. However, these schemes are not robust and non-physical overshoots and undershoots may occur. Hence, the high-resolution scheme option, which maintains the blend factor as close as possible to unity without violating the boundedness principle, was chosen. In the present simulations, non-physical overshoots or undershoots in the solution were not encountered. Convergence criterion was fixed at residuals root mean square (RMS) value lower than 10^{-4}. The low Grashof numbers encountered during the entire course of simulations justified laminar flow conditions.

6. Results and discussion

6.1. Calculation of wall heat flux

At representative time steps, heat fluxes at the walls (sidewall, top and bottom surfaces) were determined using the CFX post processor. The wall heat flux at any given height on the curved surface is related to the temperature gradient by the following equation:

$$q_w = k \left.\frac{\partial T}{\partial r}\right|_{r=R} \tag{6}$$

Temperature depends on both r and z and increases towards the curved wall, i.e. with increasing radial coordinate r. The heat transfer coefficient is defined as follows:

$$q_w = h(T_w - T_{\text{bulk}}) \tag{7}$$

6.2. Estimation of suitable bulk temperature

Bird et al. (2002) observe that care should be taken to note the definitions of the heat transfer coefficients when using treatises and handbooks. Many literature sources do not clearly define the heat transfer coefficients. To obtain the heat transfer coefficient from the heat flux (Eq. (7)), it is necessary first to define the reference or 'bulk' temperature (T_{bulk}). For flow past submerged bodies, the bulk fluid temperature may be set as that of the infinite surroundings. For fluid flow through a conduit, cup mean

Please cite this article in press as: Kannan, A., Sandaka, P.C.G., Heat transfer analysis of canned food sterilization in a still retort, Journal of Food Engineering (2008), doi:10.1016/j.jfoodeng.2008.02.007

mixing temperatures are often used. However, for the natural convection engendered flow within the confines of a food can, the fluid flow is circulatory. However, the cup mean mixing temperature would not apply at a given cross section because the net flow across the cross section would be zero. Hence, it is possible to define a bulk temperature in terms of absolute mass flow averaged temperature ($\langle T^{M}\rangle$) as given below

$$\langle T^{M}\rangle = \frac{\int_0^R |v|_z Tr\,dr}{\int_0^R |v|_z r\,dr} \tag{8}$$

The heat flux from the vertical curved wall was estimated. Horizontal slice planes, across which the flow occurs, are constructed at different locations along the curved wall. Nine equidistant slice planes are used and these are located at 11.11 millimeter intervals along the curved wall of the regular cylinder. The influence of the top and bottom walls would be minimal especially for long cylinders. However, a similar procedure, by constructing vertical planes, may not be adopted for estimating the local heat transfer coefficients at the top and bottom surfaces of the can. For this case, the method is fraught with uncertainties associated with heat transfer contributions not only from the top and bottom walls but from the curved wall as well. The temperature field would be influenced by heat flux from the curved wall as well as from the top and bottom surfaces. This effect would be significant especially when the diameter of the cylinder is small relative to the height, i.e. for high aspect ratios. It would be then incorrect to calculate the local heat transfer coefficient based only on the heat flux contribution from the bottom or top surface. Hence, a more convenient definition of the heat transfer coefficient is necessary and it will be interesting to compare its predictions with the earlier proposed method.

It is also possible to base the mean heat transfer coefficient on the volume-averaged temperature in the domain. The volume-averaged temperature is the temperature that would be obtained if the entire contents of the can were to be mixed. The volume-averaged temperature is defined as shown below

$$\langle T^{V}\rangle = \frac{\int\int\int_V Tr\,dr\,d\theta\,dz}{\int\int\int_V r\,dr\,d\theta\,dz} \tag{9}$$

The heat transfer coefficients results based on both these methods are presented and compared in the next section.

6.3. Heat transfer coefficient based on the absolute mass flow averaged temperature

The local heat transfer coefficient (h^{M}) was estimated using Eq. (8) after constructing the horizontal slice planes as discussed in Section 5.3. Its variation along the axial direction is plotted for different time steps as illustrated in Fig. 1. In this figure, it may be seen that each time step the heat transfer coefficient is nearly a constant along the vertical direction. There is a small increase near the top and bottom walls due to heat transfer effects from these surfaces. The decline in heat transfer coefficients with time may be attributed to leveling of temperature gradients in the domain. This in turn was caused by conduction and natural convective mixing. The heat transfer coefficient varied from an initial value of nearly 500 W/m^2 °C to only 40 W/m^2 °C at the final stages of the heating process.

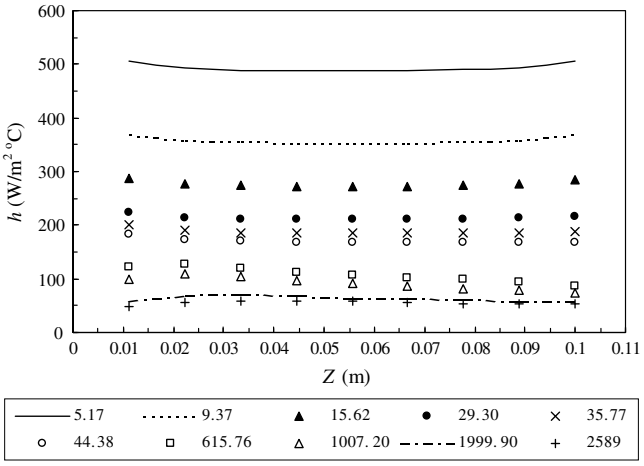

Fig. 1. Variation of the local heat transfer coefficients at different times (in seconds).

The axially averaged heat transfer coefficient based on the absolute mass flow averaged temperature (h^{M}_{avg}) is defined by

$$h^{M}_{avg} = \frac{\int_0^L h^{M}\,dz}{L} \tag{10}$$

This averaged heat transfer coefficient is shown in Fig. 2 as a function of time.

6.4. Heat transfer coefficient based on the volume averaged temperature

The method outlined earlier required a tedious procedure of evaluating heat transfer fluxes at different locations and calculating the absolute mass flow averaged temperature at each plane. The advantage is that it enables the prediction of local heat transfer coefficients, which however in the present case do not vary significantly along the axial direction (Fig. 1). A more convenient method would be to evaluate the total heat flux into the cylinder at any given time instant. The average heat transfer coefficient may then be estimated in terms of the volume-averaged temperature according to

$$q^{V}_{avg} = h^{V}_{avg}(T_{wall} - \langle T^{V}\rangle) \tag{11}$$

The volume averaged heat transfer coefficient (h^{V}_{avg}) is compared with the absolute mass flow averaged heat transfer coefficient (h^{M}_{avg}) in Fig. 2. It is interesting to note from this figure that volume averaged heat transfer coefficients are in reasonable agreement with those estimated earlier based on the absolute mass flow averaged temperatures. The reason for this effect is analyzed next.

Please cite this article in press as: Kannan, A., Sandaka, P.C.G., Heat transfer analysis of canned food sterilization in a still retort, Journal of Food Engineering (2008), doi:10.1016/j.jfoodeng.2008.02.007

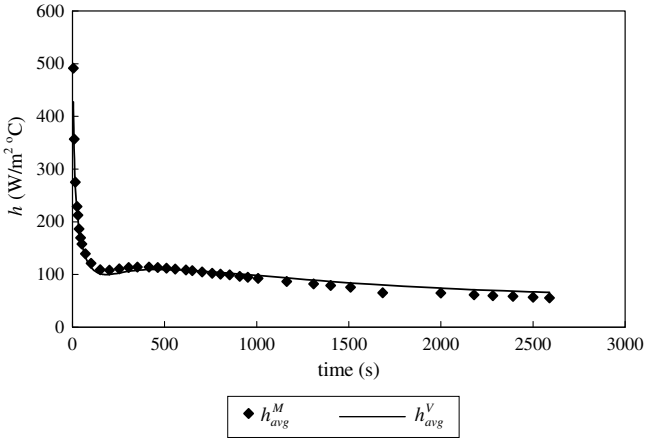

Fig. 2. Comparison of average heat transfer coefficients based on average absolute mass flow average and volume averaged temperatures.

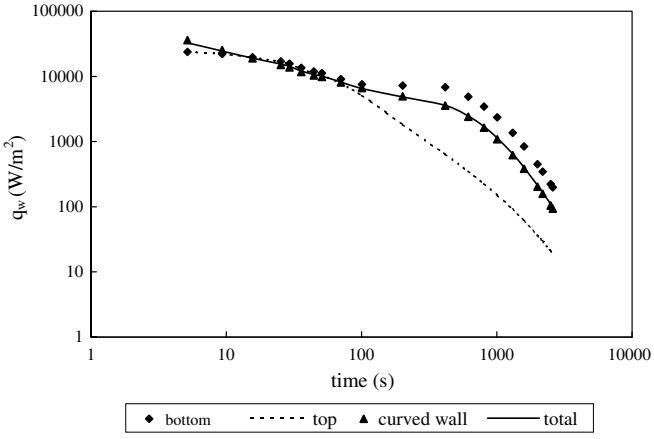

Fig. 3. Variation of heat flux with time at the top, bottom and curved surfaces and their total contribution.

The average heat transfer flux from the curved walls (q_{avg}) is based on the average of the product of the heat transfer coefficient and the temperature driving force. Expressing the heat flux at any given time instant in terms of $\langle T^M \rangle$ and averaging along the vertical direction leads to the following expression for the averaged heat flux (q^M_{avg})

$$\begin{aligned} q^M_{avg} &= \overline{h^M (T_w - \langle T^M \rangle)} \\ &\approx h^M_{avg} \overline{(T_w - \langle T^M \rangle)} \end{aligned} \tag{12}$$

The over bar is used to denote the averaging along the axial direction to distinguish it with the earlier averages represented by the symbol '⟨ ⟩'. Usually the average of product of two quantities is not the same as the product of the averages of the individual quantities. However, in the present case approximation to Eq. (12) was made possible since there was not too much of a variation of the local heat transfer coefficient (h^M) along the axial direction (Fig. 1). As the wall temperature is maintained constant, the above equation may be expressed as

$$q^M_{avg} = h^M_{avg} (T_w - \overline{\langle T^M \rangle}) \tag{13}$$

This equation may be compared with Eq. (11) where the averaged heat transfer coefficient was based on volume average temperature. These two equations may now be used to analyze why the volume averaged heat transfer coefficient that considers the entire domain is close to the absolute mass flow averaged heat transfer coefficient that is only based on the curved surface. The contributions to the total heat flux from the curved, bottom and top surfaces were analyzed. The surface groups' option in CFX enables the estimation of heat transfer fluxes either from individual surfaces or from their combination. The results are shown in Fig. 3.

Initially the contributions to the heat flux from the three surfaces are uniform. However, with increasing time, the heat flux from the top wall surface declines rapidly due to attainment of higher temperatures inside the can at the upper regions. The heat flux from the bottom wall is even more than the total heat flux. The total heat flux is an average value based on the sum of heat transfer rates from all the three surfaces divided by the total area. This coincides more or less with the heat flux from the curved wall. While the heat flux from the bottom wall alone appears to dominate, it is to be noted that its effect would be lower on the heat transfer rates since the surface area of the bottom surface is only 18.22% of the curved surface (see Fig. 3). From Fig. 3 it is observed that the total heat flux may be well represented by the contribution from the curved surface. Hence q^M_{avg} will be close to q^V_{avg}. From Eqs. (11) and (13) it may be inferred that for the heat transfer coefficients h^M_{avg} and h^V_{avg} to be comparable, the axial average of mass flow averaged temperature ($\overline{\langle T^M \rangle}$) should be close to the volume averaged value ($\langle T^V \rangle$). As the azimuthal variation in the absolute mass flow averaged temperature is negligible owing to axisymmetry, averaging this temperature along the axial direction of the can would lead to a value that is close to the volume averaged temperature ($\langle T^V \rangle$). This has been verified as illustrated in Fig. 4 over the entire duration of the thermal sterilization process.

6.5. Estimation of heat transfer rates from the surfaces

The heat transfer rates from the top, curved and bottom surfaces were compared at different time instants. From each of the surface groups created earlier and the converged results, the heat transfer flux, area and heat transfer rate could be calculated. The heat transfer rate contributions from the three surfaces as well as the total heat transfer rate are depicted in Fig. 5 as a function of time. While the rate of energy transfer to the cylindrical segment initially was around 100 W, it declines by two orders of magnitude near the end of the sterilization process. Until the first 80 seconds, the bottom and top surfaces contributed almost equally to the total heat transfer rate. Later however, the heat transfer rates decline substantially, especially from the top surface. Differences persist between the two significant heat transfer surfaces viz. the bottom surface

Please cite this article in press as: Kannan, A., Sandaka, P.C.G., Heat transfer analysis of canned food sterilization in a still retort, Journal of Food Engineering (2008), doi:10.1016/j.jfoodeng.2008.02.007

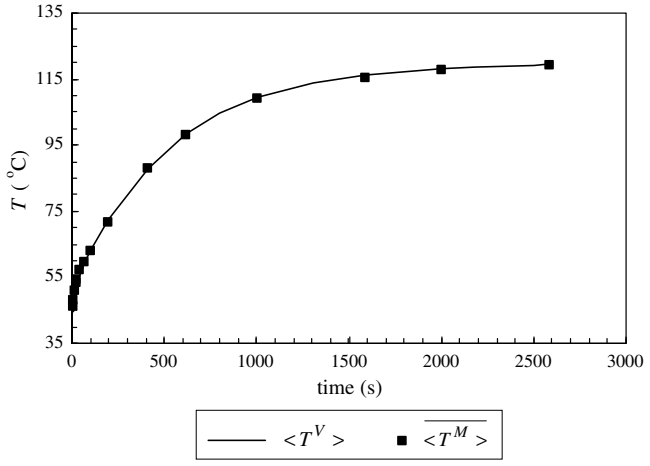

Fig. 4. Comparison between the volume average temperature and axial average of the absolute mass flow average temperature.

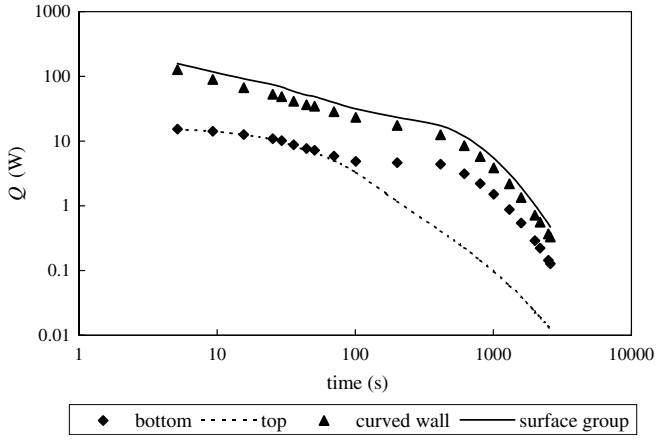

Fig. 5. Comparison of heat transfer rates from the top, bottom and curved surfaces of the food can and their total contribution.

and the curved sidewall with the latter dominating. In this context, any innovations to enhance the thermal sterilization process would require concentrating on the curved sidewall of the cylinder rather than the top or bottom walls or to device means through which heat transfer from the top and bottom surfaces may be improved. It is interesting to note that Varma and Kannan (2006) observed that a cone pointing upwards (CNU) provided significant heat transfer enhancement over a cylinder and even more so than a cone pointing downward (CND). The CNU arrangement would totally obviate the heat transfer from the top while the CND arrangement gives predominance to it thereby leading to poor performance.

6.6. Nusselt number analyses

The heat transfer coefficients based on the volume-averaged temperatures were expressed in the Nusselt number form using cylinder length (L) as the characteristic dimension. Different thermal conductivities of the food medium were also considered in the analyses to investigate their effect on the heat transfer process. The Nusselt number (Nu) variation with Rayleigh number (Ra) was first determined with the latter defined as follows:

$$Ra = \frac{g\beta\rho L^3\langle\Delta T\rangle}{\langle\mu\rangle\alpha_T} \tag{14}$$

Plotting the Nusselt numbers directly as a function of the Rayleigh numbers for different cylinders and thermal conductivities led to peculiar trends as shown in Fig. 6. Two Nusselt number values are possible for the same Rayleigh number in the region where the branches overlap. For a given aspect ratio (S), the Nusselt number curve is located at lower values of Rayleigh number at higher thermal conductivities. For a given thermal conductivity, the curve is shifted towards higher Rayleigh number values at higher aspect ratios. These imply that heat penetration into the can would take a longer time to complete at higher aspect ratios and smaller thermal conductivities. The Nusselt number trends were analyzed next by focusing on the volume-averaged quantities such as the temperature driving force ($\langle\Delta T\rangle$), fluid medium viscosity ($\langle\mu\rangle$) and their ratio ($\langle\Delta T\rangle/\langle\mu\rangle$). At lower times, when compared to $\langle\Delta T\rangle$, $\langle\mu\rangle$ decreases more rapidly leading to the initial increase in $\langle\Delta T\rangle/\langle\mu\rangle$. Subsequently, $\langle\Delta T\rangle$ tends to zero while $\langle\mu\rangle$ attains a nearly constant value of 3.4 Pa s thereby producing a declining trend in $\langle\Delta T\rangle/\langle\mu\rangle$ ratio. Hence a maximum is observed in the plot of $\langle\Delta T\rangle/\langle\mu\rangle$ with time. These are illustrated for the regular cylinder case with food medium thermal conductivity of 0.7 W/m °C in Figs. 7–9. Other cylinders exhibited similar trends.

For a fixed can aspect ratio and food medium thermal conductivity, the maximum in $\langle\Delta T\rangle/\langle\mu\rangle$ is a characteristic property of the food medium as it gets heated gradually. This maximum correlated with the product of the thermal conductivity and aspect ratio as shown

$$\left(\frac{\langle\Delta T\rangle}{\langle\mu\rangle}\right)_{max} = 8.22(kS)^{0.144} \tag{15}$$

The correlation coefficient value for this fit was 0.99.

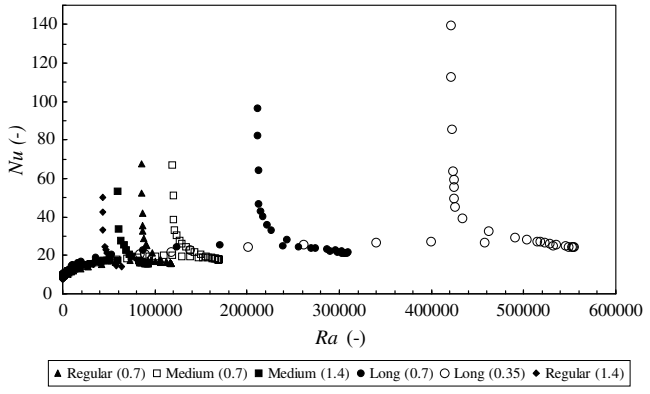

Fig. 6. Variation of Nusselt number with Rayleigh number at different aspect ratios. Food medium thermal conductivities W/m °C are shown in parentheses.

Please cite this article in press as: Kannan, A., Sandaka, P.C.G., Heat transfer analysis of canned food sterilization in a still retort, Journal of Food Engineering (2008), doi:10.1016/j.jfoodeng.2008.02.007

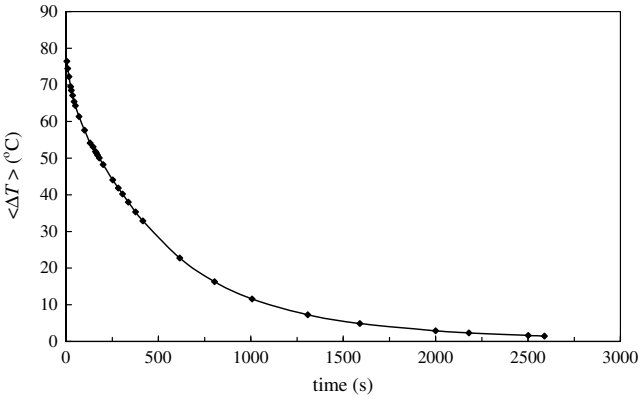

Fig. 7. Variation of volume averaged temperature driving force ($\langle \Delta T \rangle$) with time for the regular cylinder with food thermal conductivity of 0.7 W/m °C.

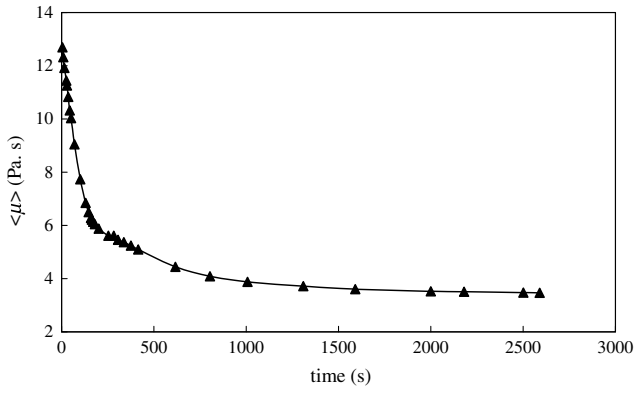

Fig. 8. Variation of volume averaged viscosity with time for the regular cylinder with food thermal conductivity of 0.7 W/m °C.

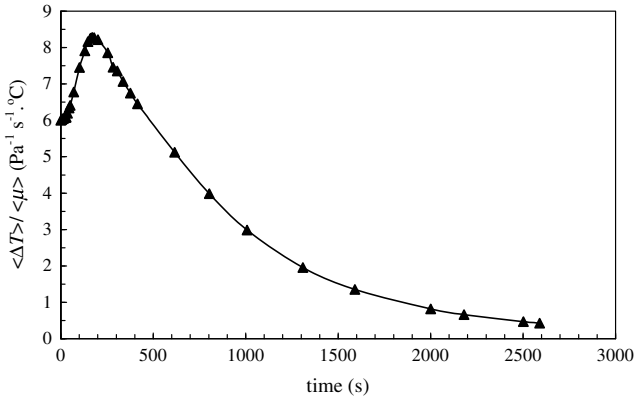

Fig. 9. Variation of $\left(\frac{\langle \Delta T \rangle}{\langle \mu \rangle}\right)$ with time for the regular cylinder with food thermal conductivity of 0.7 W/m °C.

The $\left(\frac{\langle \Delta T \rangle}{\langle \mu \rangle}\right)$ values for each of the cans may be scaled by its corresponding maximum value to yield the reduced $\left(\frac{\langle \Delta T \rangle}{\langle \mu \rangle}\right)_r$. The empirical fit to variation of $\left(\frac{\langle \Delta T \rangle}{\langle \mu \rangle}\right)_r$ with Fourier number $\left(Fo = \frac{\alpha t}{R^2}\right)$ is given by

$$\left(\frac{\langle \Delta T \rangle}{\langle \mu \rangle}\right)_r = \frac{1.58 \exp(-11.15 Fo)}{1 + 1.42 \exp(-74.84 Fo)} \tag{16}$$

The deviation (absolute) of the model prediction from the CFD value was divided by the CFD value to give the absolute relative deviation. The average value of such deviations was reported as the average absolute relative deviation (AARD). The AARD for the predictions from Eq. (16) was estimated to be 13.7%. However if the Fourier numbers corresponding to very high heating times were not considered, the AARD reduced to 7.7%.

The critical Fourier number corresponding to the maximum value of $\left(\frac{\langle \Delta T \rangle}{\langle \mu \rangle}\right)_r$ may be determined by setting the first derivative of Eq. (16) with respect to Fourier number to zero. This leads to a critical Fourier number (Fo_c) of 0.028. Since heat transfer data are expressed commonly in terms of Rayleigh number rather than by $\left(\frac{\langle \Delta T \rangle}{\langle \mu \rangle}\right)$, the Rayleigh number dependency on Fourier number is next determined.

Since the Rayleigh numbers covered a wide range of values (300–5.5×10^5) as was shown in Fig. 6, it was also necessary to scale the Rayleigh number. For each can-thermal conductivity combination, the maximum Rayleigh number (Ra_{max}) was obtained from the corresponding value of $\left(\frac{\langle \Delta T \rangle}{\langle \mu \rangle}\right)_{max}$. Hence, defining Ra_{max} as

$$Ra_{max} = \frac{g\beta L^3 \left(\frac{\langle \Delta T \rangle}{\langle \mu \rangle}\right)_{max} \rho}{\alpha_T} \tag{17}$$

the individual Rayleigh number values were scaled to give the reduced Rayleigh number as given in

$$Ra_r = \frac{Ra}{Ra_{max}} \tag{18}$$

The Fourier number values were also scaled by dividing with the critical Fourier number to yield the reduced Fourier number (Fo_r). The reduced Rayleigh number correlated

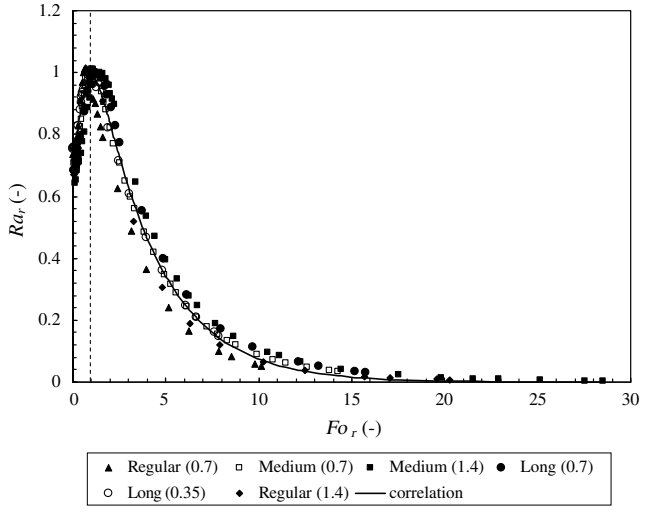

Fig. 10. Variation of reduced Rayleigh number with reduced Fourier number for food cans of different aspect ratios and thermal conductivities. The dashed line indicates the critical reduced Fourier number.

Please cite this article in press as: Kannan, A., Sandaka, P.C.G., Heat transfer analysis of canned food sterilization in a still retort, Journal of Food Engineering (2008), doi:10.1016/j.jfoodeng.2008.02.007

with Fo_r as given in Eq. (19) and the fit with the data are shown in Fig. 10.

$$Ra_r = \frac{1.18\exp(1.72Fo_r)}{1+0.75\exp(2.02Fo_r)} \tag{19}$$

The critical reduced Fourier number is shown by the dashed line. The average absolute relative deviation (AARD) was estimated to be 13%. However if the data corresponding to very high heating times ($Fo_r > 10$) were not considered, the AARD reduced to 7.5%. The Fourier number is the primary variable for correlating $\left(\frac{\langle \Delta T\rangle}{\langle \mu\rangle}\right)_r$ and Nu. However, in natural convection literature, the Nusselt number is correlated usually in terms of the Rayleigh number. As shown in Eq. (19), there is an explicit relation between the reduced Rayleigh number and reduced Fourier numbers. The decision to use the reduced Fourier number directly or in combination with the reduced Rayleigh number will be governed by the trends exhibited by the data in the different heat transfer regimes. These will be discussed next in the development of correlations for Nusselt number.

Two Nusselt number regimes, classified as sub critical and supercritical were defined, depending on whether the

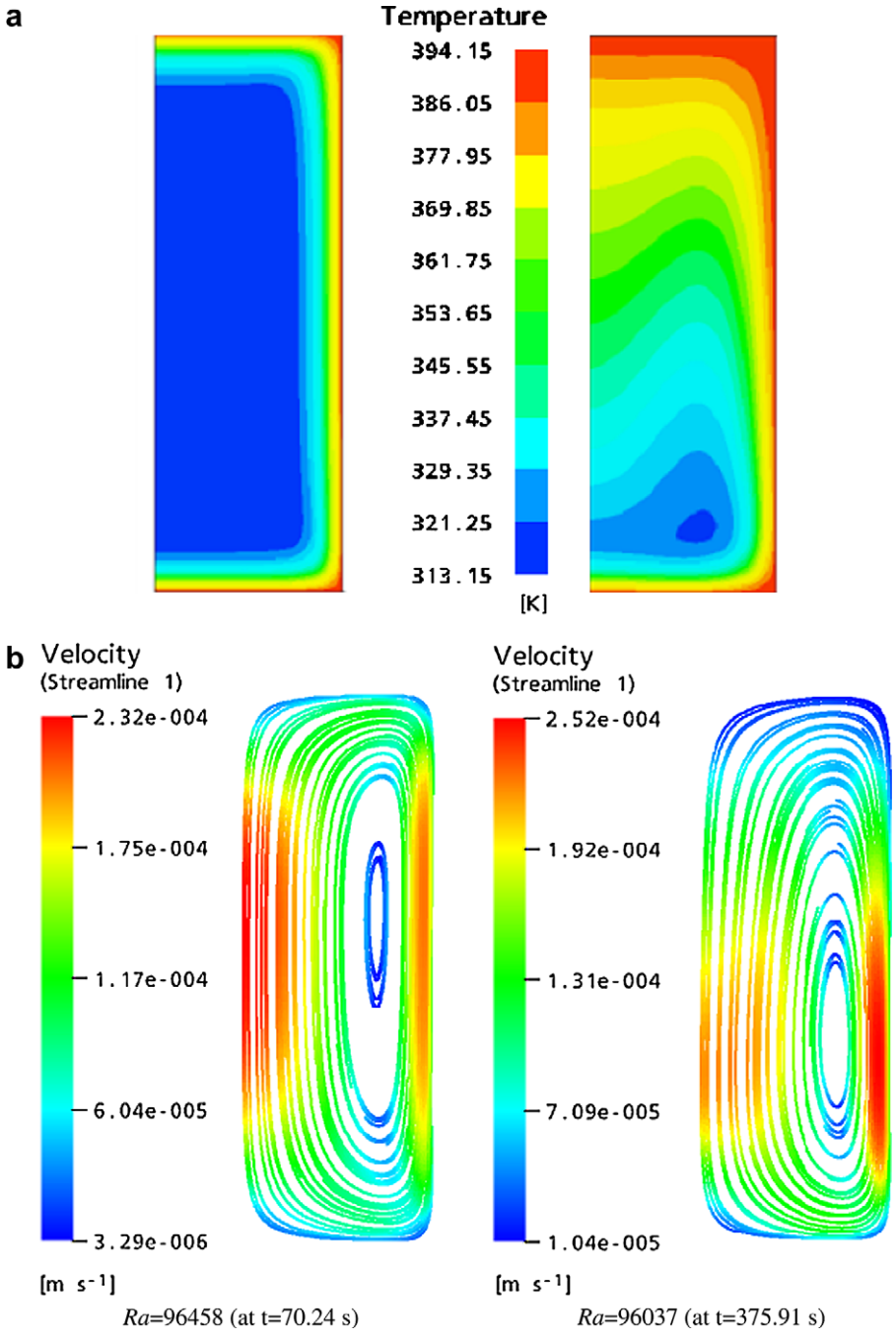

Fig. 11. Temperature contours (a) and streamline patterns (b) at nearly the same Rayleigh number but at different times for the regular cylinder with food medium thermal conductivity of 0.7 W/m °C.

Please cite this article in press as: Kannan, A., Sandaka, P.C.G., Heat transfer analysis of canned food sterilization in a still retort, Journal of Food Engineering (2008), doi:10.1016/j.jfoodeng.2008.02.007

Fo_r was less than or greater than unity. This was necessary in view of the type of the dominant heat transfer mechanism prevalent in these two regimes. The temperature contours and streamlines plots in the sub-critical and supercritical regimes for approximately the same Rayleigh numbers for the regular cylinder case are shown in Fig. 11a and b. It may be inferred from these figures that in the sub-critical regime, the heat transfer is mainly by conduction with uniform Kernels of temperature zones. In the supercritical regime, the convection currents contort the temperature profiles.

6.6.1. Sub critical regime

The Nusselt number data that were defined in terms of the can length (L) as the characteristic dimension were rescaled by dividing with the aspect ratio (S). The scaled Nusselt number (Nu_S) is defined as shown in

$$Nu_S = \frac{Nu}{S} = \frac{h\frac{L}{k}}{\frac{L}{D}} = h\frac{D}{k} \tag{20}$$

The scaled Nusselt number will lead to the characteristic dimension being diameter of the cylinder rather than its length. In the sub critical regime, the scaled Nusselt number data was correlated as follows:

$$Nu_S = \frac{8.92}{Fo_r^{0.45}} \tag{21}$$

The correlation fit is reasonable for a wide range of Fourier numbers, thermal conductivities and aspect ratios. In order to facilitate comparison with the theoretical prediction, this correlation may be expressed in terms of actual Fourier number as follows:

$$Nu_S = \frac{1.78}{Fo^{0.45}} \tag{22}$$

The plot in terms of the actual Fourier number is given in Fig. 12. The average absolute relative deviation (AARD) was estimated to be 4.7%.

In the conduction dominated heat transfer regime, the Nusselt number by definition becomes unity. Further, from the heat conduction equation, we have

$$\frac{\partial T}{\partial t} = \alpha_T \frac{\partial^2 T}{\partial r^2} \tag{23}$$

From scaling analysis described by Bejan (1995), it may be shown that if $r \sim \delta_T$, where δ_T is the conduction layer thickness, the above equation will become

$$\frac{\Delta T}{t} \approx \alpha_T \frac{\Delta T}{\delta_T^2} \tag{24}$$

This results in the following relation for δ_T

$$\delta_T \approx \sqrt{\alpha_T t} \tag{25}$$

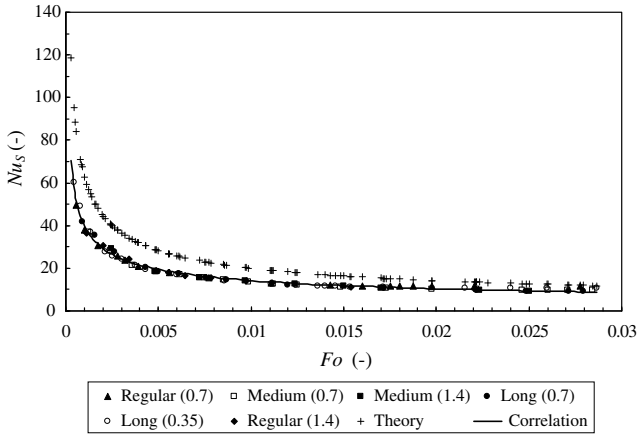

Fig. 12. Correlation for Nusselt number in the sub critical regime.

Using the definition of the Fourier number, this equation becomes

$$\delta_T \approx \frac{D}{2}\sqrt{Fo} \tag{26}$$

Hence using the conduction layer thickness as the true characteristic dimension for conduction-dominated situations, the definition for Nusselt number becomes

$$Nu_C = h\frac{\delta_T}{k} = 1 \tag{27}$$

Hence

$$Nu_C = h\frac{\frac{D}{2}\sqrt{Fo}}{k} = 1 \tag{28}$$

Hence the scaled Nusselt number given by theory (Nu_S^*) is given by

$$Nu_S^* = h\frac{D}{k} = \frac{2}{\sqrt{Fo}} \tag{29}$$

This simplified expression is shown in comparison with the actual correlation prediction (Eq. (22)) and CFD data in Fig. 12. While the trend is captured by the theoretical model (Eq. (29)), its predictions are however higher than the actual correlation (Eq. (22)). The reason may be that the radial propagation of the conductive heat flux may have been inhibited by the onset of axial convection currents that carry away the heat in a direction perpendicular to the direction of conductive heat transfer. In any case for $Fo_r < 1$, the conduction mechanism is the dominant if not the sole mechanism of heat transfer. The discrepancy in the exponent, which deviated from 0.5, was further analyzed. It was observed that a marginally better correlation fit could be obtained by expressing the scaled Nusselt number as

$$Nu_S = \frac{a}{Fo_r^{0.5-bRa_r}} \tag{30}$$

This correlation was proposed to account for the effects of convection on the Fourier number exponent. For the range of Rayleigh numbers studied, the modified exponent to Fo_r

Please cite this article in press as: Kannan, A., Sandaka, P.C.G., Heat transfer analysis of canned food sterilization in a still retort, Journal of Food Engineering (2008), doi:10.1016/j.jfoodeng.2008.02.007

(as well as *Fo*) ranged only between 0.44 and 0.46. Hence, the simpler form given by Eqs. (21) and (22) was retained.

6.6.2. Supercritical regime

The analysis in this regime is complicated since the simple conduction heat transfer is no longer dominating. Natural convection currents would influence the temperature profile strongly as shown in Fig. 11. In addition, the conduction effects may be still important at supercritical Fourier numbers not much higher than unity. The variation of Nusselt number with the reduced Fourier number in the supercritical regime is shown in Fig. 13. It may be inferred that more than the thermal conductivity, it is the aspect ratio that is playing a key role. It may be seen that for long cylinders with twice the variation in thermal conductivities, the Nusselt numbers are nearly the same. There is a minor effect of thermal conductivity especially before the peak. The trend suggests that lower the thermal conductivity value, higher the Nusselt number. Higher the aspect ratio, higher is the Nusselt number. This figure also indicates, that the Nusselt number first *increases* before decreasing with increasing Fourier number, a trend distinct enough not to be ignored. The simple scaling of the Nusselt number, which unified the data in the sub critical regime, failed in the supercritical regime. The maximum in the Nusselt number was correlated to the aspect ratio and thermal conductivity as shown below

$$Nu_{\max} = 12.84\frac{S^{0.69}}{k^{0.18}} \tag{31}$$

The correlation coefficient value for this fit was 0.98. Using this correlation, the Nusselt numbers in the supercritical regime were reduced by dividing with $Nu_{\max}$. The trend of the reduced Nusselt number passing through a maximum may be modeled as a combination of two effects, of which one would vanish at higher Fourier numbers. In the modeling process, the reduced Rayleigh number was also used since the trends showed a monotonic variation with this variable at higher Fourier numbers as would be expected in natural convective processes.

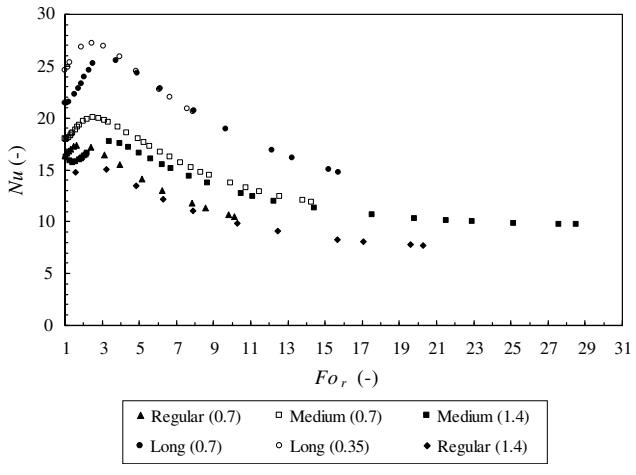

Fig. 13. Variation of Nusselt number with reduced Fourier number in the supercritical regime.

Martynenko and Khramtsov (2005) propose a similar approach involving both Fourier and Rayleigh numbers for transient two dimensional heat transfer inside a completely filled horizontal cylinder at aspect ratios exceeding 2.5. There are both similarities and differences between their work and the present study. These authors defined a Fourier number range (0–Fo_1) in the transient period, where Fo_1 was correlated with the Rayleigh number at initial time (Ra_{d0}) as follows:

$$Fo_1 = 0.4Ra_{d0}^{0.25} \tag{32}$$

A function f was defined in the Prandtl number range 0.7–25, as shown below

$$f(Pr) = 1 - 0.21\exp(-0.247Pr) \tag{33}$$

The Nusselt number was defined by

$$Nu_{hc} = \frac{0.279f(Pr)Ra_{d0}^{0.15}}{Fo[Fo^{-0.575} - 0.486f(Pr)Ra_{d0}^{0.25}]} \tag{34}$$

The authors also identified a quasi steady state regime, where the Rayleigh number (Ra_d) ranged between 10^5 and 10^{10} in which the Nusselt number could be correlated as follows:

$$Nu_{hc} = 0.59Ra_d^{0.25} \tag{35}$$

Similar to the present study, the heat transfer coefficients decreased rapidly followed by a much slower decrease (Fig. 2). However, their correlations are not applicable to the present case where the cylinder alignment is vertical. The aspect ratios would be drastically different for the horizontal orientation of the cylindrical food can. Further the Prandtl numbers encountered in the present work (10^4–1.5×10^5) are much higher than the range specified for their correlations. However, the correlations show that both Fourier numbers and Rayleigh numbers are necessary to model the Nusselt number even though the Rayleigh number itself depends on the Fourier number. The simple nature of this dependency (Eq. (32)) in contrast to the present case (Eq. (19)) also indicates that the fluids behavior in the two analyses is different. In addition, the effect of aspect ratio is not present in these correlations. However, the Nusselt number is shown to be a monotonic function of Rayleigh number in the quasi steady state regime.

In the proposed approach, the Nusselt number may be modeled in terms of a convective term, which is solely a function of the Rayleigh number and a conductive heat transfer correction to it that is applicable at values close to the critical Fourier number. The conductive heat transfer correction would vanish rapidly at high values of supercritical Fourier numbers. The following correlation was fitted to the data

$$Nu_r = 1.05Ra_r^{0.16} - 0.2\frac{Ra_r^{7.96}}{Fo_r^{0.5}} \tag{36}$$

Please cite this article in press as: Kannan, A., Sandaka, P.C.G., Heat transfer analysis of canned food sterilization in a still retort, Journal of Food Engineering (2008), doi:10.1016/j.jfoodeng.2008.02.007

The second term becomes insignificant at higher Fourier numbers that correspond to lower values of the reduced Rayleigh number (see Fig. 15). Hence, it may be seen that at higher Fourier numbers, the Nusselt number simplifies to

$$Nu_r = 1.05Ra_r^{0.16} \tag{37}$$

The correlation produces a fit within ± 10% to the CFD numerical data.

6.7. Validation of temperatures and heat flux data obtained from CFD

Numerical calculations for laminar flow CFD simulations are straightforward, as the governing transport equations do not pose additional complications. This is in contrast to turbulent flow where additional model equations are required to provide closure (Srinivasan et al., 2005). Hence, the error may arise mainly from numerical discretization of the time and space domains. The sufficiency of the discretization steps were verified through mesh and time step independency studies. To the best of our knowledge, information in form of experimental data and empirical correlations for heat fluxes are not available for the transient natural convection flow situations in enclosed containers and non-Newtonian food systems encountered in thermal food sterilization. As described in Section 4, experiments were conducted with a test system to validate the CFD temperature predictions. The midpoint location was chosen for measurement to avoid end and wall effects. The measured temperatures were found to be in reasonable agreement with the CFD predictions as shown in Fig. 14.

Next, the mean Nusselt number values obtained from CFD simulations of the actual model system was validated. If the vertical wall of the cylinder is approximated as an isothermal plate, then an appropriate literature correlation for Nusselt number may be used for at least an order of magnitude comparison. For natural convective heat transfer into a non-Newtonian fluid flowing steadily past an isothermal vertical surface the following correlation for the mean Nusselt number has been suggested (Skelland, 1967; Chhabra and Richardson, 1999)

$$Nu_{VP} = C_{nc}(Gr_{VP})^{\frac{1}{2(n+1)}}(Pr_{VP})^{\frac{n}{3n+1}} \tag{38}$$

where the Grashof and Prandtl number definitions for a vertical plate are given as follows:

$$Gr_{VP} = \frac{\rho^2 L^{n+2}[g\beta(T_w - T_0)]^{2-n}}{K^2} \tag{39}$$

$$Pr_{VP} = \frac{\rho C_P}{k}\left(\frac{K}{\rho}\right)^{\frac{2}{1+n}} L^{\frac{1-n}{1+n}}(Lg\beta(T_w - T_0))^{\frac{3(n-1)}{2(1+n)}} \tag{40}$$

In Eqs. (39) and (40), K refers to the fluid consistency index of the power law fluid. It is taken as the product of μ_0 and the exponential temperature dependent term given in Table 1 for the model system. K was evaluated at the film temperature, which was defined as the arithmetic mean of the wall and bulk flow temperature. In the present analysis, the bulk flow temperature was chosen as the volume-averaged temperature. The temperature T_0 used in Eqs. (39) and (40) refer to the temperature outside the thermal boundary layer. For flow past a flat plate, this temperature would be the bulk fluid temperature. For flow inside the cylindrical can, T_0 is taken as the volume averaged temperature. The constant C_{nc} in Eq. (38) was 0.636 for the model system. The CFD based Nusselt numbers based on the volume averaged heat transfer coefficients (h^V_{avg}) were compared with Eq. (38) for the regular cylinder at two different food medium thermal conductivities (Fig. 15). It may be observed that the correlation fit to CFD data is not good initially when conduction is the dominant mechanism. In the conduction-dominated sub critical regime, the Nusselt number trend followed the analytical expression (Eq. (29)) as discussed in Section 6.6. However, a reasonable fit may be observed later when the convection effects are established inside the can. The flat plate correlation will increasingly apply for food cans of large radii and low food medium thermal conductivities as shown in Fig. 15b.

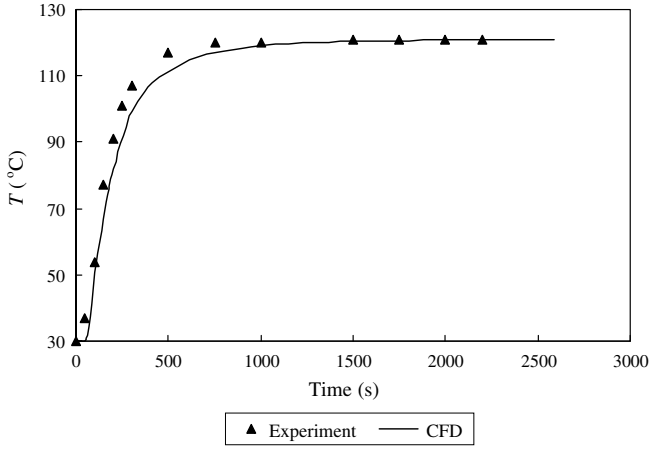

Fig. 14. Comparison between experimentally measured and CFD predicted midpoint temperatures.

6.8. Estimation of the volume averaged temperatures

To predict the total heat flux from Eq. (11), the heat transfer coefficient (h^V) and volume-averaged temperature $\langle T\rangle$ are necessary. The heat transfer coefficient in the sub critical and supercritical regimes may be estimated from the Nusselt number correlations (Eqs. (21) and (36)). As suggested by one of the anonymous reviewers, the volume-averaged temperature at any time instant may be estimated by integrating the following lumped parameter model for transient heat transfer

$$\rho V C_p \frac{d\langle T\rangle}{dt} = h^V A(T_w - \langle T\rangle) \tag{41}$$

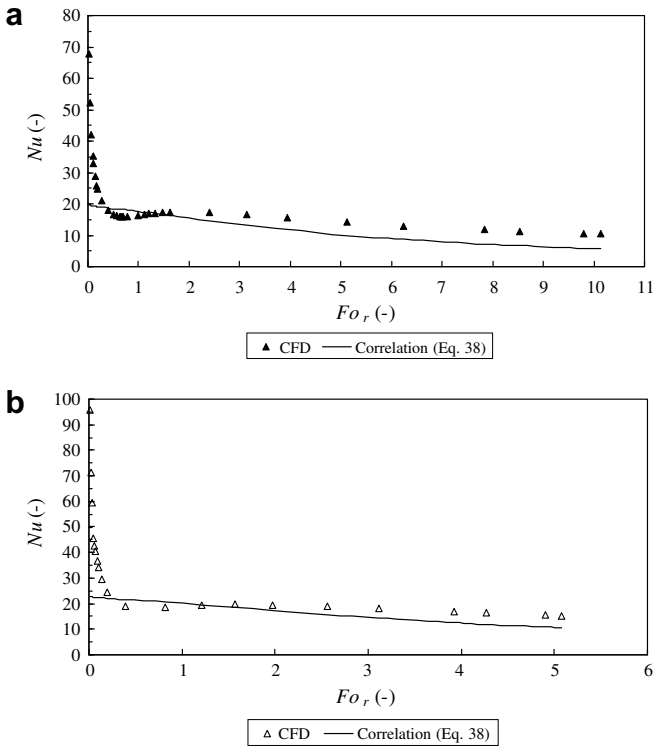

Fig. 15. Comparison of CFD predicted mean Nusselt numbers for the regular cylinder with the correlation for the flat plate (a) $k = 0.7$ W/m °C (b) $k = 0.35$ W/m °C.

6.8.1. Sub critical regime ($Fo_r \leqslant 1$)

From Eqs. (20) and (21), the heat transfer coefficient (h^V) may be expressed as a function of Fo_r. The resulting expression may be integrated to yield the following analytical expression for the volume-averaged temperature

$$\langle T \rangle = T_w - (T_w - T_0) \exp\left(-0.454\left(\frac{S+0.5}{S}\right) Fo_r^{0.55}\right) \quad (42)$$

After substituting the values for the wall temperature and initial temperature, the above equation gives the volume-averaged temperature in Kelvin as

$$\langle T \rangle = 394.15 - 81 \exp\left(-0.454\left(\frac{S+0.5}{S}\right) Fo_r^{0.55}\right) \quad (43)$$

When the volume-averaged temperatures from this equation were compared with those predicted from CFD, the agreement was not too bad. A maximum temperature difference of about 2 °C was observed at $Fo_r = 1$. However, when initiating the calculations in the supercritical regime ($Fo_r > 1$), this temperature offset would lead to further errors that carry over when estimating $\langle T \rangle$ at different times in the supercritical regime. Hence, an alternative was sought to predict temperatures better in the sub critical regime.

As discussed in Section 6.6 and illustrated in Fig. 11a, this regime is characterized by conduction dominated heat transfer. Hence, the temperature in the domain may be estimated from the analytical solution of the two-dimensional transient heat conduction equation. Using the product solution method described in Holman (1997), the temperature $T(r,z)$ in the finite cylinder of length L and radius R may be obtained by taking the product of the solutions for the infinite cylinder of radius R and the infinite flat plate of thickness L. The resulting expression is given by

$$\frac{T - T_0}{T_w - T_0} = 1 - \frac{8}{\pi} \sum_{m=1}^{\infty} \sum_{n=1}^{\infty} \frac{(-1)^{m+1}}{(2m-1)} \times \cos\left(\frac{2m-1}{L}\pi z\right) \frac{J_0\left(\gamma_n \frac{r}{R}\right)}{\gamma_n J_1(\gamma_n)} \times \exp\left[-\left(\frac{2m-1}{L}\right)^2 \pi^2 \alpha t\right] \exp\left(-\gamma_n^2 \frac{\alpha t}{R^2}\right) \quad (44)$$

where γ_n is Bessel root of the function

$$J_0(\gamma)_n = 0 \quad (45)$$

where J_0 and J_1 are Bessel functions of orders zero and one respectively. The solutions to Eq. (45) are given in standard mathematical handbooks or may be obtained from MATLAB® calculations. These solutions apply for the case when the external surface heat transfer coefficient is very high. This is justified in the present analyses as condensing steam is used as the heating medium. Eq. (44) may be volume averaged using the form of Eq. (9) to obtain the following relation

$$\frac{\langle T \rangle - T_0}{T_w - T_0} = 1 - \frac{32}{\pi^2} \sum_{m=1}^{\infty} \sum_{n=1}^{\infty} \frac{1}{[(2m-1)\gamma_n]^2} \times \exp\left[-\left(\frac{2m-1}{L}\right)^2 \pi^2 \alpha t\right] \exp\left(-\gamma_n^2 \frac{\alpha t}{R^2}\right) \quad (46)$$

The volume-averaged temperatures in the sub critical regime were predicted using Eq. (46) and were found to be in reasonable agreement with the CFD predictions (Table 3). Especially at $Fo_r = 1$, the difference between the volume-averaged temperatures predicted by CFD simulations and Eq. (46) was about 0.5 °C.

6.8.2. Supercritical regime ($Fo_r > 1$)

In this regime, convection has set in the cylinder and the volume-averaged temperature may be obtained using the lumped parameter approach. Using $Nu = h^V L/k$, the above equation becomes

$$\rho V C_p \frac{d\langle T \rangle}{dt} = Nu \frac{k}{L} A (T_w - \langle T \rangle) \quad (47)$$

In the supercritical regime, direct analytical integration is not possible because the Nusselt number is a function of Rayleigh number in addition to time (Eq. (36)). The Rayleigh number (Ra) in turn, is a function of the can dimensions, time (or equivalently Fo_r) and the temperature driving force (ΔT). These dependencies are shown in Eqs. (17)–(19). The Nusselt number (Nu) is obtained by multiplying its reduced form (Nu_r) with Nu_{max} using Eq. (31). Estimates of $\langle T \rangle$ in the supercritical regime were then

Please cite this article in press as: Kannan, A., Sandaka, P.C.G., Heat transfer analysis of canned food sterilization in a still retort, Journal of Food Engineering (2008), doi:10.1016/j.jfoodeng.2008.02.007

Table 3
Volume-averaged temperature predictions in the subcritical and supercritical regimes

No.	Time (s)	Medium can (0.7 W/m °C)		
		Fo_r (–)	$\langle T\rangle_{CFD}$ (K)	$\langle T\rangle_{model}$ (K)
1	15.62	0.0861	323.64	324.13
2	40.074	0.2209	330.00	330.30
3	72.391	0.3990	335.45	335.66
4	112.14	0.6181	340.45	340.53
5	159.65	0.8800	345.30	345.09
6	181.4175	1.00	347.38	346.88
7	**201.02**	**1.1080**	**349.04**	**348.65**
8	**305.46**	**1.6837**	**357.42**	**357.46**
9	**454.55**	**2.5055**	**367.17**	**367.74**
10	**566.15**	**3.1207**	**372.75**	**373.48**
11	**896.49**	**4.9415**	**382.92**	**383.76**
12	**1308.8**	**7.2142**	**388.59**	**389.39**
13	**1509.9**	**8.3227**	**390.54**	**390.79**
14	**1798.6**	**9.9140**	**391.47**	**392.06**
15	**2078**	**11.4541**	**392.31**	**392.78**
16	**2589**	**14.2708**	**393.17**	**393.47**

The supercritical regime values are shown in bold.

obtained by numerically integrating Eq. (47) with the ODE45 routine of MATLAB®. The initial value for $\langle T\rangle$ is provided at a time corresponding to $Fo_r = 1$ using the analytical conduction solution prediction Eq. (46). The predictions based on the methods for both regimes are shown in Table 3. A good match between the volume-averaged temperatures obtained from the lumped parameter model and CFD simulations may be observed.

7. Summary and conclusions

CFD analyses provide insight on the thermal sterilization process in relatively long food cans of different aspect ratios. Two different methods were used to define and estimate the heat transfer coefficient. The volume averaged temperature based definition of the heat transfer coefficient is more convenient to use relative to the absolute mass flow averaged heat transfer coefficient. The heat flux and heat transfer rate contributions from the different surfaces of the food can are different. The curved surface, owing to its larger surface area especially for cylinders with high aspect ratio, dominates the heat transfer process.

The Nusselt numbers exhibited a sharp decrease with time. The *Nu–Ra* plot indicated branching at high Rayleigh numbers. This was attributed to the ratio of volume-averaged temperature driving force to viscosity group exhibiting a maximum as it varied with time. The critical Fourier number at which the $\langle \Delta T\rangle/\langle \mu\rangle$ value attained maximum was estimated. A unified correlation was developed for the reduced Rayleigh number as a function of reduced Fourier number.

The Nusselt number seemed to be governed essentially by conduction based mechanism in the sub-critical Fourier number range. Nusselt number analysis in the sub critical regime indicated that the aspect ratio switched the characteristic dimension from a length scale to a diameter scale. This is mainly due to conductive heat transfer in the radial direction. However, in the supercritical Fourier number range, the Nusselt number was increasingly governed by natural convection. Correlations were developed for the Nusselt number both in the sub critical and supercritical regions.

The application of CFD techniques in predicting temperature variation with time was validated experimentally using a test system. The CFD derived Nusselt numbers were also validated with an available literature correlation developed for isothermal plates. A reasonable match was observed in the convection-dominated regime especially at low food medium thermal conductivity. The volume-averaged temperatures were estimated reasonably from the analytical solution in the conduction dominated sub critical regime and the lumped parameter model in the supercritical regime.

The present work may find applications in thermal sterilization optimal control studies where the energy consumption is incorporated into the objective function. Previous studies mainly apply optimization strategies on the much simpler conduction model, which may not be realistic for convection heated liquid foods. The correlations developed may be used to estimate the heat transfer fluxes as a function of time, which upon integration will lead to estimation of energy consumption.

Acknowledgement

The simulations were carried out form the facilities given by the Centre for Computational Fluid Dynamics, Indian Institute of Technology Madras, Chennai 600 036.

References

Bird, R.B., Stewart, W.E., Lightfoot, E.N., 2002. Transport Phenomena, second ed. John Wiley, New York.

Bejan, A., 1995. Convection Heat Transfer, second ed. John Wiley, New York.

Can Manufacturers Institute, Washington. (<http://www.cancentral.com>).

Catton, I., 1978. Natural convection in enclosures. In: Proceedings of the Sixth International Heat Transfer Conference, vol. 6, Toronto, Canada, pp. 13–31.

CFX, 2003 Documentation, CFX Ansys Ltd., Didcort, Oxfordshire, UK.

Chhabra, R.P., Richardson, J.F., 1999. Non-Newtonian Flow in the Process Industries. Butterworth–Heinemann, Oxford.

Datta, A.K., Teixeira, A.A., 1987. Numerical modeling of natural convection heating in canned liquid foods. Transactions of American Society of Agricultural Engineers 30 (5), 1542–1551.

Datta, A.K., Teixeira, A.A., 1988. Numerically predicted transient temperature and velocity profile during natural convection heating of canned liquid foods. Journal of Food Science 53 (1), 191–195.

Dewitt, D.P., Incropera, F.P., 2001. Fundamentals of Heat and Mass Transfer, fifth ed. John Wiley, New York.

Engelman, M., Sani, R.L., 1983. Finite element simulation of an in-package pasteurization process. Numerical Heat Transfer 6, 41–54.

Farid, M.M., Ghani, A.G.A., 2004. A new computational technique for the estimation of sterilization time in canned food. Chemical Engineering and Processing 43, 43–51.

Ghani, A.G.A., 2006. A computer simulation of heating and cooling liquid food during sterilization process using computational fluid dynamics. Association for Computing Machinery New Zealand Bulletin, 2(3), ISSN: 1176-9998.

Ghani, A.G.A., Farid, M.M., Chen, X.D., Richards, P., 1999. Numerical simulation of natural convection heating of canned food using computational fluid dynamics. Journal of Food Engineering 41, 55–64.

Ghani, A.G.A., Farid, M.M., Chen, X.D., 2002a. Theoretical and experimental investigation of the thermal inactivation of *Bacillus stearothermophilus* in food pouches. Journal of Food Engineering 51, 221–228.

Ghani, A.G.A., Farid, M.M., Chen, X.D., 2002b. Theoretical and experimental investigation of the thermal destruction of vitamin C in food pouches. Computers and Electronics in Agriculture 34, 129–143.

Ghani, A.G.A., Farid, M.M., Chen, X.D., 2002c. Numerical simulation of transient temperature and velocity profiles in a horizontal can during sterilization using computational fluid dynamics. Journal of Food Engineering 51, 77–83.

Ghani, A.G.A., Farid, M.M., Zarrouk, S.J., 2003. The effect of can rotation on the thermal sterilization of liquid food using computational fluid dynamics. Journal of Food Engineering 57, 9–16.

Gourisankar, S.P.Ch., 2006. Heat transfer analysis in canned food sterilization. M. Tech. Project Report, IIT Madras.

Holman, J.P., 1997. Heat Transfer, eighth ed. McGraw-Hill, New York.

Kumar, A., Bhattacharya, M., Blaylock, J., 1990. Numerical simulation of natural convection heating of canned thick viscous liquid food product. Journal of Food Science 55 (5), 1401–1411.

Kumar, A., Bhattacharya, M., 1991. Transient temperature and velocity profiles in a canned non-Newtonian liquid food during sterilization in a still-cook retort. International Journal of Heat and Mass Transfer 34 (4–5), 1083–1096.

Marra, F., Romano, V., 2003. A mathematical model to study the influence of wireless temperature sensor during assessment of canned food sterilization. Journal of Food Engineering 59 (2–3), 245–252.

Martynenko, O.G., Khramtsov, P.P., 2005. Free Convective Heat Transfer. Springer, New York.

Naveh, D., Kopelman, I.J., Pflug, I.J., 1983. The finite element method in thermal processing of foods. Journal of Food Science 48, 1086.

Neeharika, K., 2007. CFD simulations and experimental analysis of canned food sterilization. M.Tech. Project Report, IIT Madras.

Nicolai, B.M., Verboven, B., Scheerlinck, N., De Baerdemacker, J., 1998. Numerical analysis of the propagation of random parameter fluctuations in time and space during thermal food processes. Journal of Food Engineering 38, 259–278.

Rhie, C.M., Chow, W.L., 1983. Numerical study of the turbulent flow past an airfoil with trailing edge separation. AIAA Journal 21, 1527–1532.

Skelland, A.H.P., 1967. Non-newtonian Flow and Heat Transfer. Wiley, New York.

Srinivasan, R., Jayanti, S., Kannan, A., 2005. Effect of Taylor vortices on mass transfer from a rotating cylinder. AIChE Journal 51 (11), 2885–2898.

Steffe, J.F., Mohamed, I.O., Ford, E.W., 1986. Rheological properties of fluid foods: data compilation. In: Okos, M.R. (Ed.), Physical and Chemical Properties of Foods. American Society of Agricultural Engineering, St. Joseph, MI.

Teixeira, A.A., Dixon, J.R., Zahradnik, J.W., Zinsmeister, G.E., 1969. Computer optimization of nutrient retention in thermal processing of conduction-heated foods. Food Technology 23 (6), 134–140.

Varma, M.N., Kannan, A., 2005. Enhanced food sterilization through inclination of the container walls and geometry modifications. International Journal of Heat and Mass Transfer 48 (18), 3753–3762.

Varma, M.N., Kannan, A., 2006. CFD studies on natural convective heating of canned food in conical and cylindrical containers. Journal of Food Engineering 77, 1024–1036.

Zechman, L.G., Pflug, I.J., 1989. Location of the slowest heating zone for natural convection heating fluids in metal containers. Journal of Food Science 54, 205–229, 226.

Please cite this article in press as: Kannan, A., Sandaka, P.C.G., Heat transfer analysis of canned food sterilization in a still retort, Journal of Food Engineering (2008), doi:10.1016/j.jfoodeng.2008.02.007